Phys. Status Solidi C **9**, No. 5, 1296–1302 (2012) / **DOI** 10.1002/pssc.201100195

physica status solidi c
www.pss-c.com
current topics in solid state physics

Quantum dynamics of damped and driven anharmonic oscillators

Michael Schrapp[*,1], **Elena del Valle**[2], **Jonathan J. Finley**[1,2], **and Fabrice P. Laussy**[1]

[1] Walter Schottky Institute, Technical University Munich, Am Coulombwall, 85748 Garching, Germany
[2] Physikdepartment, Technical University Munich, Am Coulombwall, 85748 Garching, Germany

Received 27 May 2011, accepted 20 February 2012
Published online 12 April 2012

Keywords anharmonic oscillator, coherent excitation, four wave mixing

* Corresponding author: e-mail michaelschrapp@yahoo.de

We study various techniques to characterize the quantum states of a strongly dissipative system, namely, the anharmonic oscillator. One cannot directly access the quantum states themselves but only transitions between them. Various methods bring various advantages and inconvenients. We compare several observables under coherent and incoherent excitation. Incoherent excitation leads to huge broadening while coherent excitation quickly dresses the system at the energies required to access the excited states. Less perturbative methods such as four wave mixing appear to be superior but are, by construction, only usable for the lowest rungs.

1 Introduction The physics of light-matter coupling in nanostructures [1] is a privileged arena where to realize and study fundamental quantum physics, with the hope of applications and large scale integration. Because semiconductors are typically noisy systems with large decay rates, a dissipative description is often necessary. The interplay of quantum dynamics and decay leads to complicated interferences between the quantum states [2], which can only be accessed through transitions between poorly defined eigenenergies, making it often problematic to probe the structure of such systems.

Here, we consider the quantum dynamics of a dissipative anharmonic oscillator, arguably the simplest nontrivial system of this type. The anharmonic system represents a fundamental theoretical problem by itself, with applications in different fields of quantum optics, solid state physics, molecular and atomic physics [1-3]. It is, for instance, a popular model to describe interacting polaritons in microcavities [4,5]. Advantages and disadvantages of various techniques to probe this quantum optical system are presented; we undergo a comprehensive analysis of the anharmonic oscillator, considering coherent versus incoherent excitation, as well as a more elaborate technique — Four Wave Mixing (FWM) — recently developed to access dressed states in the Jaynes–Cummings model [11, 12].

We study the Hamiltonian (with $\hbar = 1$ throughout the paper)

$$H = \omega_a a^\dagger a + V a^{\dagger 2} a^2 \tag{1}$$

ω_a is the intrinsic mode frequency, a and $a^\dagger$ the boson annihilation and creation operators and V is the anharmonic (quadratic) term. Diagonalizing H, which can be done exactly, leads to the transition frequencies $\omega_n = E_n - E_{n-1} = \omega_a + 2V(n-1)$, in terms of the eigenfrequencies of the system:

$$E_n = \omega_a n + V(n-1)n \tag{2}$$

We will consider $\omega_a = 0$ as the reference energy without loss of generality. Figure 1 shows the energy levels of the system. To compute all the quantities of interest, we use the Lindblad master equation formalism

$$\frac{d\rho}{dt} = \mathcal{L}\rho = -i[H,\rho] + \frac{\gamma}{2}\mathcal{L}_a\rho \tag{3}$$

where $\mathcal{L}_a\rho = 2a\rho a^\dagger - a^\dagger a\rho - \rho a^\dagger a$. Dissipation with a decay rate of γ is included.

An important observable in our study is the photoluminescence (PL) spectrum. In the steady state (taken at $t = 0$) it reads,

$$S(\omega) = \frac{1}{\pi n_a^{SS}} \int_0^\infty e^{i\omega\tau} \langle a^\dagger(0) a(\tau)\rangle d\tau\,, \tag{4}$$

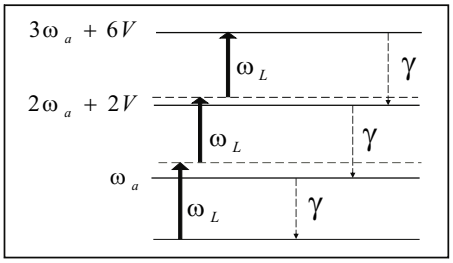

Figure 1 Energy level diagram of the first three transitions of the anharmonic oscillator. A 3-photon resonance is depicted where 3 photons from a probe laser, with frequency ω_L, hit the third rung. The dashed arrows indicate dissipation in the system with loss rate γ.

in terms of the two-time correlator $\langle a^\dagger(0)a(\tau)\rangle$, which can be obtained through the quantum regression theorem.

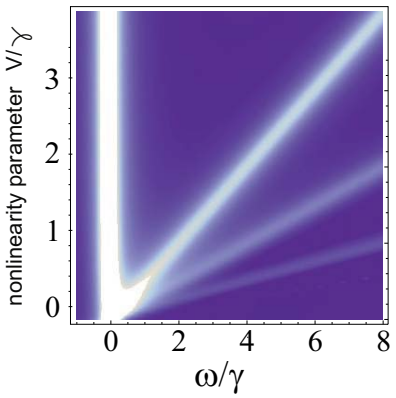

Figure 2 Density plot of the PL spectrum in the steady state under incoherent excitation as a function of frequency ω and anharmonic parameter V. Increasing the parameter V yields to larger transition frequencies. The different lines correspond to different rungs of the anharmonic ladder.

2 Incoherent excitation Typical examples of incoherent pumping in semiconductors are continous wave excitation or electrical injection in the wetting layer. Both provide an incoherent and continuous income of excitation. It is described, as noted before, through the pumping Lindblad term $\frac{P}{2}(2a^\dagger\rho a - aa^\dagger\rho - \rho aa^\dagger)$ in the dissipative master equation.

We introduce the number state $|n\rangle$ with n excitations in the system and calculate the density matrix elements

$$\frac{d}{dt}\langle n|\rho|m\rangle = \langle n|\left(-i[H,\rho] + \frac{\gamma}{2}\mathcal{L}_a\rho + \frac{P}{2}\mathcal{L}_{a^\dagger}\rho\right)|m\rangle \tag{5}$$

in this basis. The probability of having n excitations in the system, $p(n) = \langle n|\rho|n\rangle$, can be obtained from Eq. (5).

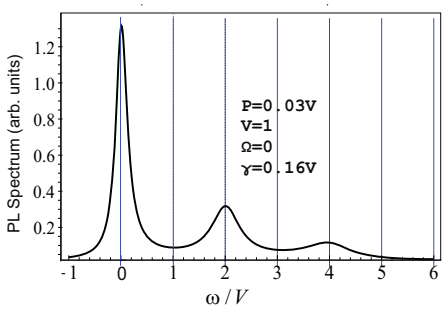

Figure 3 PL spectrum in the steady state under incoherent excitation in units of V (a cut of Fig. 2 at $V = 1$). Transitions from the first three rungs are visible and allow to identify properly the dressed states that gave rise to them.

Its equation reduces, in the steady state under incoherent pumping, to:

$$\frac{d}{dt}p(n) = 0 = -[n\gamma + (n+1)P]p(n) + nPp(n-1) + (n+1)\gamma p(n+1)\,. \tag{6}$$

The solution is a thermal field independently of the anharmonicity V (which should always remain $V \ll \omega_a$):

$$p(n) = \left(\frac{P}{\gamma}\right)^n \frac{\gamma - P}{\gamma}\,. \tag{7}$$

The corresponding average population of the cavity reads

$$n_a = \langle a^\dagger a\rangle = \sum_n np(n) = \frac{P}{\gamma - P}\,, \tag{8}$$

and the single time, second order correlation function

$$g^{(2)}(0) = \frac{\sum_n n(n-1)p(n)}{n_a^2} = 2\,. \tag{9}$$

Because n_a and $g^{(2)}(0)$ are independent of V, we can not extract any information about the system from these quantities. One has to look into spectral observables, related to the eigenenergies, in order to understand the impact of the anharmonicity under incoherent excitation. The change in the PL spectrum when varying V is apparent in the density plot of Fig. 2. In Fig. 3, we make a cut of this plot at $V = 1$ where one can clearly identify the transitions from the first three rungs.

3 Coherent excitation To excite the system coherently, a resonant continous wave ($\Omega e^{i\omega_L t} + h.c.$) is used. This enters the dynamics in the Hamiltonian as

$$H = \omega_a a^\dagger a + Va^{2\dagger}a^2 + \Omega(ae^{i\omega_L t} + a^\dagger e^{-i\omega_L t})\,. \tag{10}$$

To get rid of the explicit time dependence, we carry out a unitary transformation into the rotating frame of the laser:

$$\tilde{H} = U^\dagger HU - iU^\dagger\frac{dU}{dt}\,, \tag{11}$$

with $U = e^{-i\omega_L a^\dagger a t}$. The operators a and $a^\dagger$ evolve under the operator U as $\tilde{a}(t) = e^{i\omega_L t}a$ and $\tilde{a}^\dagger(t) = e^{-i\omega_L t}a^\dagger$, respectively. Inserting this into the Hamiltonian (10) gives:

$$\tilde{H} = \Delta a^\dagger a + \Omega(a + a^\dagger)\,, \tag{12}$$

where we have defined the detuning to the laser frequency $\Delta = \omega - \omega_L$.

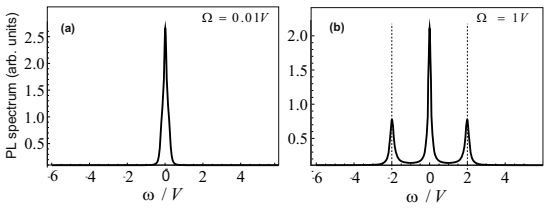

Figure 4 PL spectrum in the steady state under coherent excitation resonant with the first rung ($\Delta = 0$). In (a) we have a very low intensity of the laser and thus get only 1 peak at the laser frequency $\omega = \omega_L$. In (b) we increase the intensity and a Mollow triplet arises.

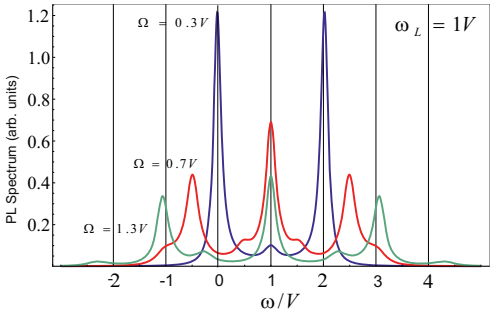

Figure 5 PL spectrum in the steady state under coherent excitation in the two photon absorption regime (that is, resonant with the second rung, $2\omega_L = \omega_1 + \omega_2$, or $\Delta = V$). At small pumping power ($\Omega < 0.3V$) the transition from the second to the first rung is visible (blue curve, at $\omega = 0, 2$). But for high excitation power dressed states gets created and the features intrinsic to the systems are more difficult to extract.

3.1 PL spectrum Let us start by probing the system with a coherent laser resonant with the first rung, that is $\Delta = 0$, and look at the PL spectrum. Figure 4 shows the dressing of this rung by the laser, that manifests as a Mollow triplet. The side peaks lie exactly at the "Mollow" frequencies $\omega_{\text{Mollow}} = \pm\sqrt{(2\Omega)^2 - (\frac{\gamma}{4})^2}$. Excitation at frequency $\omega_L = V$ yields a two photon absorption, and for high excitation power also dressed states appear (Fig. 5).

In the simplest case of the harmonic oscillator, the different transitions cannot be resolved in the PL spectrum. The quantized nature of the quantum oscillator is completely washed out due to the driving of the laser. To analyse this phenomenon theoretically, we study first the time dependent physical spectrum. Following the definition of Eberly and Wódkiewicz [10], the time dependent spectrum can be written as:

$$S(t,\omega) = \iint_0^t e^{-(\frac{\Gamma}{2} - i\omega(t-t_1)} e^{-(\frac{\Gamma}{2} + i\omega(t-t_2)} \times \langle a^\dagger(t_1)a(t_2)\rangle dt_1 dt_2\,. \tag{13}$$

Neglecting the linewidth of the detector, $\Gamma = 0$, performing a variable transformation, and using $\langle a^\dagger(t_2)a(t_1)\rangle = \langle a^\dagger(t_1)a(t_2)\rangle^*$, we obtain the normalized physical spectrum:

$$S(t,\omega) = \frac{2\Re\int_0^t dT \int_0^{t-T} e^{i\omega\tau}\langle a^\dagger(T)a(T+\tau)\rangle d\tau}{\int_0^t \langle a^\dagger(T)a(T)\rangle dT}. \tag{14}$$

Next, we consider the evolution of the physical spectrum after the laser has turned on at $t = 0$. Figure 6 shows the physical spectrum at two different times. One clearly sees two peaks, at ω_L and $\omega_a = 0$, corresponding to the intrinsic frequencies of two interacting elements, laser and harmonic mode. In the limit $t \to \infty$ the second peak vanishes and the time dependent spectrum converges to the common laser-type delta function.

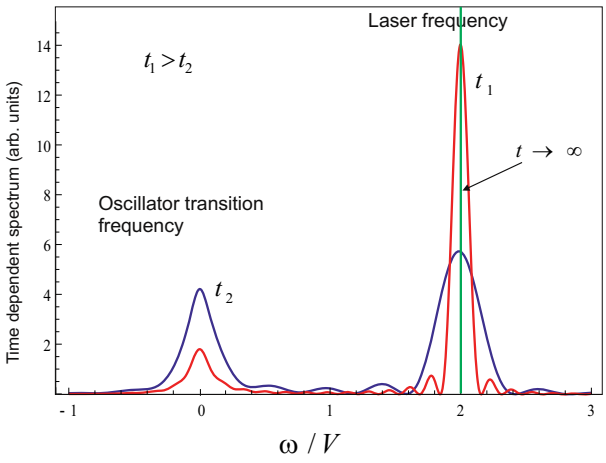

Figure 6 Time dependent physical spectrum of the harmonic oscillator. At short times, two peaks (at the laser frequency and at the transition frequency) are clearly visible. After some time, the laser drives the system to its own (laser) frequency and thus the transition frequency is washed out from the spectra.

3.2 Population and higher order correlation functions In the steady state, the population $n_a = \langle a^\dagger a\rangle$ of the anharmonic mode is a meaningful quantity to observe the multi photon absorption at frequencies $\frac{E_n}{n} = \omega_a + V(n-1)$, see Fig. 7. Increasing the laser intensity, higher rungs of the anharmonic ladder get probed (Fig. 8), though we learned from the discussion that the intensity should not be so high that dressed states appear in the system.

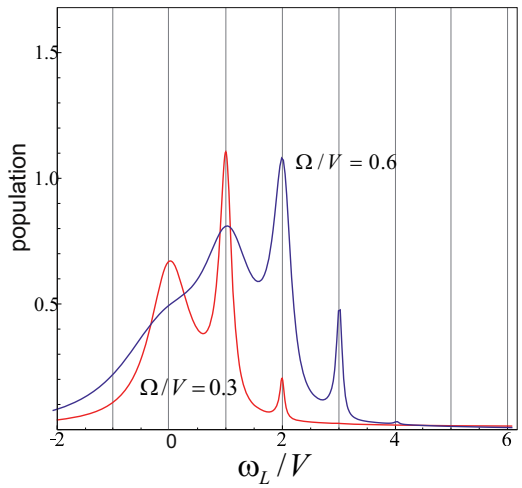

Figure 7 Population of the cavity as a function of laser frequency ω_L for two different laser intensities. The peaks correspond to multi photon absorption. If the laser intensity increases, higher rungs of the ladder gets probed.

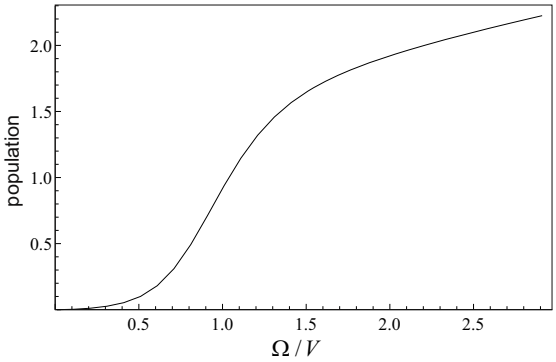

Figure 8 Population n_a as a function of laser intensity for $\omega_L = \omega_a$. The population increases monotoneously. This behaviour is qualitatively similar for different values of ω_L

The second order correlation function $g^{(2)}$ is typically used to describe bunching or antibunching of photons. In this case, we must compute $g^{(2)}(0)$ numerically, in contrast to incoherent pumping, because coherent pumping leads to a large number of off-diagonal elements in the density operator. The second order correlation function can be generalized to nth order:

$$g^{(n)}(0) = \frac{\langle a^{\dagger n} a^n \rangle}{n_a^n} . \tag{15}$$

Figure 9(a) shows strong features in the correlation functions with coherent excitation at the nth photon resonances. As shown with the population, higher rung get probed by increasing the laser intensity, but using higher order correlation functions than $g^{(2)}$, features of higher rungs can be displayed even with the same laser intensity (Fig. 9(a)). In addition to the previous chapter, we also can find the dressing of the system by the laser in this case, see Fig. 10. For high laser frequencies we see the expected photon bunching, but below a treshold the peaks split up due to dressed states and we get antibunching.

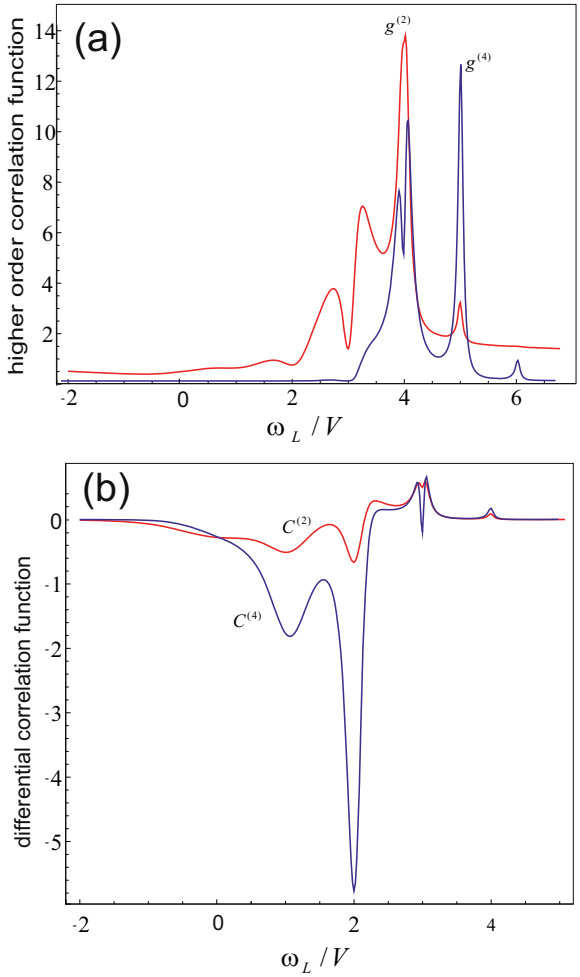

Figure 9 (a) Second and fourth order correlation functions as a function of laser frequency. $g^{(4)}$ displays information about higher rungs for the same laser intensity. (b) Second and fourth order differential correlation functions as a function of laser frequency. Both graphs show similar features. $C^{(4)}$ is scaled by a factor of $1/8000$. The laser intensity is $\Omega/V = 0.78$

Another quantity similar to $g^{(n)}$ is the differential correlation function

$$C^{(n)} = \langle a^{\dagger n} a^n \rangle - \langle a^\dagger a \rangle^n \tag{16}$$

which is popular in describing photon statistics [9]. In our case of an anharmonic oscillator there is no noticeable difference between the different orders of the $C^{(n)}$, which is shown in Fig. 9(b).
But the differential correlation functions also nicely show the crossing from antibunching to bunched photons, as it is depicted in Figure 11. This is the same behaviour like in Fig. 10.

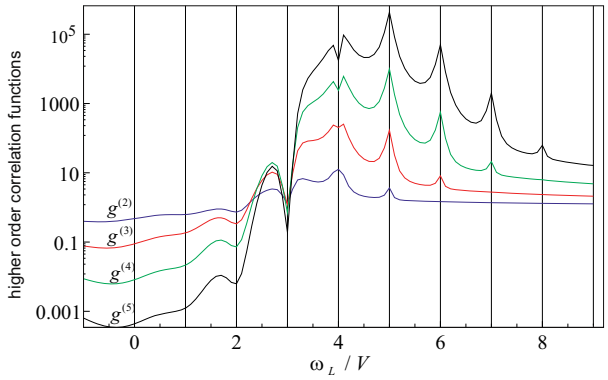

Figure 10 Logarithmic plot of correlation functions from second to fifth order with $\Omega = 0.8V$.For small ω_L the photons are antibunched, but get bunched for high enough laser frequency. At the threshold ($\omega_L = 4V$), $g^{(3)}, g^{(4)}$ and $g^{(5)}$ show antibunching, but $g^{(2)}$ already shows bunching.

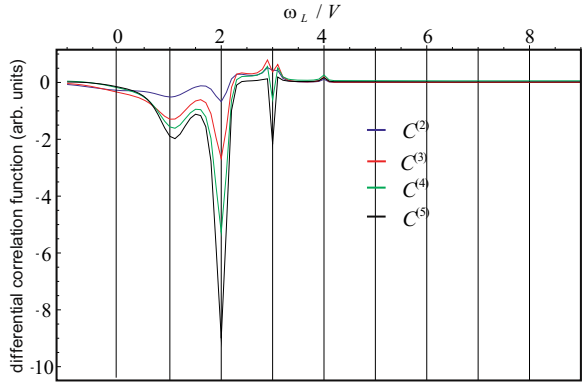

Figure 11 Differential correlation functions from second to fifth order with $\Omega = 0.8V$. They show a similar behaviour than the nth order correlation functions.

3.3 Four wave mixing (FWM) Four wave mixing is a powerful method in nonlinear (quantum) optics to observe third-order nonlinear response. The method has recently been proposed to investigate Jaynes–Cummings nonlinearities [11]. Inspired by this work, we also use here the degenerate configuration, i.e., the signal is generated via two pulses with time delay τ (Fig. 12 (a)). Following the procedure of Ref. [11], the pulses are described by adding to the Hamiltonian

$$H_{\mathrm{FWM}}(t) = E_1\delta(t+\tau)e^{i\omega_1 t}a^\dagger + E_2\delta(t)e^{i\omega_2 t}a^\dagger + h.c.\,, \tag{17}$$

where E_1, E_2 are the coupling strengths with the two pulses. A first photon at frequency ω_1 at time $-\tau$ yields to a first order polarization and two photons, each with the frequency ω_2, at time 0 produce a third order response:

$$P(t,\tau) = Tr(\rho^{(3)}(t,\tau)a)\,. \tag{18}$$

With the third order term of the density matrix

$$\rho^{(3)}(t,\tau) \propto e^{-ilt}[a^\dagger,[a^\dagger,e^{-i\mathcal{L}\tau}[a,\rho^{(0)}]]]\,. \tag{19}$$

Performing the three commutators in Eq. (19) leads to $2^3 = 8$ terms. The term $e^{-i\mathcal{L}t}(a^\dagger e^{-i\mathcal{L}\tau}\rho^{(0)}aa^\dagger)$, for example, is visualized in a quantum optics Feynman diagram (Fig. 12(b)). To evaluate Eq. (19), we need to expand the creation and annihilation operators in the photon number basis:

$$a = |0\rangle\langle 1| + \sqrt{2}|1\rangle\langle 2| + ... \tag{20}$$

$$a^\dagger = |1\rangle\langle 0| + \sqrt{2}|2\rangle\langle 1| + ... \tag{21}$$

After the first pulse, a linear polarization is generated that can be described by a first order correction to the density matrix,

$$\rho^{(1)}(-\tau) = [a,\rho^{(0)}] = -|0\rangle\langle 1|\,. \tag{22}$$

Then it evolves according to the master equation

$$\rho^{(1)}(0) = e^{-i\mathcal{L}\tau}\rho^{(1)}(-\tau)\,. \tag{23}$$

The second pulse produces a third order polarization

$$\rho^{(3)}(0) = [a^\dagger,[a^\dagger,\rho^{(0)}]] = \sqrt{2}\rho_{01}|2\rangle\langle 1|\,. \tag{24}$$

The further time evolution of $\rho^{(3)}(t,\tau)$ is again described by the master equation. We finally get:

$$P(t,\tau) = Tr(\rho^{(3)}(t,\tau)a) = \rho_{10}(t,\tau) + \sqrt{2}\rho_{21}(t,\tau). \tag{25}$$

In the following we set $\tau = 0$. From the FWM polarization in the time domain we can extract interesting features about the system, see Fig. (14). The slope of the FWM amplitude (in Log-scale) is different for short and long times evidencing the dynamics of the second and then the first rungs of the anharmonic ladder. At longer times the signal is only dominated by the first rung due to a higher dissipation rate of the second manifold.

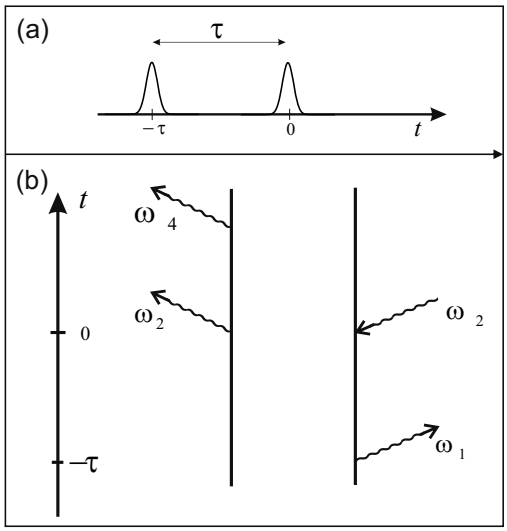

Figure 12 (a) Scheme of the temporal sequence of two pulses at times $t = -\tau$ and $t = 0$. (b) One example out of the possible 8 Feynman diagrams in the FWM. Left and right lines correspond to operators on the right and left hand side, respectively, of the initial density matrix $\rho^{(0)}$. The outgoing arrow at time $-\tau$ on the right corresponds to a annihilation of a photon and at time $t = 0$ and yields to a first order polarization. Two photons (ω_2, ω_3) at time 0 produce the third order response. Between the pulses, the system evolves freely according to the master equation.

Finally, we want to compare the FWM spectrum with the common PL spectrum under coherent and incoherent excitation. To do that, we compute

$$S_{\mathrm{FWM}}(T,\omega) = \int_T^\infty P(t,\tau)e^{i\omega t}dt\,, \qquad (26)$$

where the time integration starts with a time lag T. Figure 13 shows the FWM spectrum. The intensity of the peaks strongly depends on the time lag T. As already seen in the time domain, the intensity of the second rung decreases for a higher time lag T. By construction of the third order nonlinear response, the FWM can only show the first two rungs (Fig. 13) of the anharmonic ladder. In order to investigate higher manifolds, one needs to perform six or eight wave mixing.

4 Conclusions We considered various possibilities to probe the quantum states of a dissipative anharmonic oscillator, with coherent and incoherent excitation, as well as four wave mixing. Under incoherent excitation, transitions between many rungs of the ladder are visible in good enough systems (where quantum dynamics dominates neatly the dissipative one) but correlation functions ($g^{(2)}(0) = 2$, that is, that of thermal light) and the population do not betray any of the underlying quantum structure. These quantities become useful for that purpose under coherent excitation. The higher order correlation functions

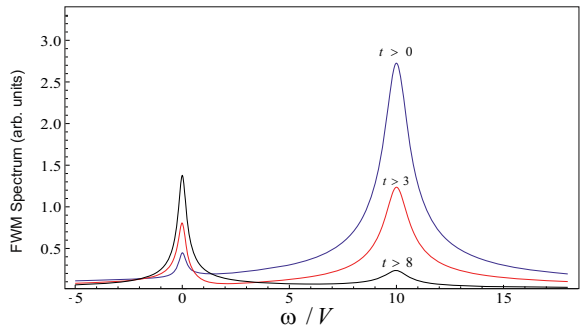

Figure 13 FWM spectrum at zero delay when varying the filtered time. It shows first and second rung transitions. First rung increases with higher time-lag

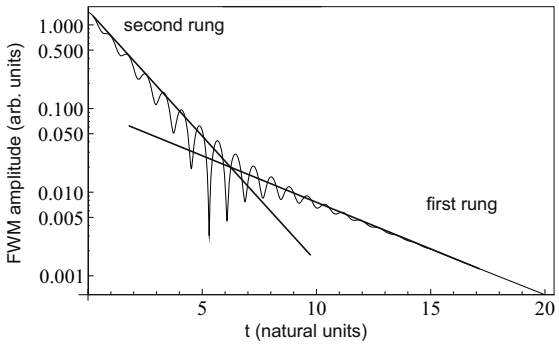

Figure 14 Amplitude of the FWM polarization at zero delay as a function of time. It shows second and then first rung dynamics.

($g^{(2)}$, $g^{(3)}$, ...) maps the system structure quite well, and better than the differential correlation functions $C^{(n)}$. High intensities of the laser to make such features more pronounced yield instead to dressing by the laser and thus the intrinsic features of the quantum anharmonic oscillator get lost. Finally, we investigated the four wave mixing method, where we have a coherent probe of the polarization, but this method is limited to the bottom of the ladder (up to second rung).

Acknowledgements DFG via SFB-631, Nanosystems Initiative Munich & EU FP-7 via SOLID and Marie Curie Initiative 'SQOD' are acknowledged for funding.

References

[1] A. Hoffmann and J. Christen, PLMCN11 conference, 2011.
[2] E. del Valle, Phys. Rev. A **81**, 053811 (2010).
[3] C. Gardiner and P. Zoller, Quantum Noise, 2nd ed. (Springer, Berlin, 2000).
[4] E. del Valle, Microcavity Quantum Electrodynamics (VDM Verlag, 2010).
[5] I. Carusotto, Phys. Rev. A **63**, 023610 (2001).
[6] E. del Valle, F. P. Laussy, F. M. Souza, and I. A. Shelykh, Phys. Rev. B **78**, 085304 (2008).

[7] T. C. H. Liew and V. Savona, Phys. Rev. Lett. **104**, 183601 (2010).
[8] E. del Valle, F. P. Laussy, and C. Tejedor, Phys. Rev. B **79**, 235326 (2009).
[9] H.J. Carmichael, Statistical Methods in Quantum Optics I, 2nd ed. (Springer, 2002).
[10] J.H. Eberly and K. Wódkiewicz, J. Opt. Soc. Am. **67**, 1252 (1977). J. H. Eberly, C. V. Kunasz and K. Wodkiewicz, J. Phys. B: At. Mol. Phys. **13**, 217 (1980).
[11] J. Kasprzak et al., Nature Mater. **9**, 304 (2010)
[12] F. P. Laussy, E. del Valle, M. Schrapp, A. Laucht, and J. Finley, arXiv:1104.3564v1.

